SELF-CONSISTENT PIC MODELING OF NEAR SOURCE TRANSPORT OF FRIB*

Chun Yan Jonathan Wong†, National Superconducting Cyclotron Laboratory, East Lansing, USA
Steven M. Lund, Kei Fukushima, Facility for Rare Isotope Beams, East Lansing, USA

Abstract

Self-consistent simulation studies of the FRIB low energy beam transport (LEBT) system are conducted with the PIC code Warp. Transport of the many-species DC ion beam emerging from an Electron Cyclotron Resonance (ECR) ion source is examined in a realistic lattice through the Charge Selection System (CSS) which employs two 90-degree bends, two quadrupole triplets, and slits to collimate non-target species. Simulation tools developed will support commissioning activities on the FRIB front end which begins early operations in 2017. Efficient transverse (xy) slice simulation models using 3D lattice fields are employed within a scripted framework that is readily adaptable to analyze many ion cases and levels of model detail. Effects from large canonical angular momentum (magnetized beam emerging from ECR), thermal spread, nonlinear focusing, and electron neutralization are examined for impact on collimated beam quality.

INTRODUCTION

The Facility for Rare Isotope Beams (FRIB) is designed to accelerate heavy ions to 200 MeV/u with 400 kW CW on target [1, 2]. The beam is produced by one of two electron cyclotron resonance (ECR) ion sources at the front end: ARTEMIS [3] and VENUS [4]. Each ion source is followed by a charge selection system (CSS) where non-target species passing the first dipole are removed in a high-dispersion region between two 90-degree dipoles. Schematics of the post-ECR and CSS lattices are embedded in Fig. 2 and 1.

Beams emerging from an ECR exhibit complex evolution because: 1) the high-current, many-species beam has strong space charge; 2) the beam is born in a high magnetic field and thus carries large canonical angular momentum; 3) the beam is partially neutralized by electrons from the ionized residual gas; and 4) the lattice is dispersive, has strong acceleration, substantial applied field nonlinearities, and fringe fields overlap for some elements. To better understand how to preserve beam brightness and optimize the CSS, a framework of code tools has been developed using the open-source PIC-code Warp [6]. This paper describes the Warp simulations (see [7, 8] for more details) and how an envelope model is employed for beam matching. Simulations contrasting the performance of the CSS under various initial beam conditions illuminate the impact of canonical angular momentum and space charge. Implications for beam collimation and further transport downstream are discussed.

* Work supported by the U.S. Department of Energy Office of Science under Cooperative Agreement DE-SC0000661 and the National Science Foundation under Grant No. PHY-1102511.
† wong@nscl.msu.edu

FRONT END MODEL IN WARP

Initial Conditions & Loading

Table 1 lists beam parameters used in the Warp simulations. An initial axisymmetric waterbag distribution adapted for space-charge [12] is injected with no centroid offset at the extraction point of the ECR. Each species' envelope extent fills the puller electrode aperture (i.e. $R_{\text{puller}} = 2\sigma_x$ where $\sigma_x^2 = \langle x^2 \rangle$). The 35kV extraction potential sets the kinetic energy of each species, and the longitudinal velocity spread and radial (thermal component) emittance arise from a 3eV ion temperature. The average canonical angular momentum of each species is set by assuming all ions are born at the same magnetic field, i.e. $\langle P_\theta \rangle = q \langle r^2 \rangle_{\text{birth}} B_{\text{birth}}/2$, where $B_{\text{birth}} = \int_{z(\text{peak 1})}^{z(\text{peak 2})} B_z(r=0)dz$ is the average axial B-field between the peaks of the solenoidal field of the ECR. Since the B-field at launch differs from B_{birth}, for $\langle P_\theta \rangle$ = const as specified, an angular velocity is injected upon each ion of the species with:

$$\theta_0' = \left[\frac{\langle r^2 \rangle_{\text{birth}}}{\langle r^2 \rangle_{\text{launch}}} B_{\text{birth}} - B_{\text{launch}} \right] / (2[B\rho]). \qquad (1)$$

Here, $[B\rho]$ is the particle rigidity, and we assume $\langle r^2 \rangle_{\text{birth}} = \langle r^2 \rangle_{\text{launch}}$. Simulated beam species and currents for U operation are given in Ref. [5].

Table 1: Beam Parameters of U^{34+} Based on VENUS

At launch	
Temperature	3 eV
$\langle P_\theta \rangle / (mc)$	0.305 mm–mrad
$\varepsilon_{r-\text{rms-norm}}$	0.015 mm–mrad
$\sigma_r = \sqrt{2}\sigma_x$	2.82 mm
$\sigma_r' = d\sigma_r/dz$	0
$\mathcal{E}$ (before/after ES Gap)	5.00 / 12.00 keV/u
$[B\rho]$ (before/after ES Gap)	7.13×10^{-2} / 1.10×10^{-1} Tm

Lattice Design & Matching Methodology

The beam line can be divided into two distinct sections: the axisymmetric transfer line from the ECR to the CSS, and the CSS which produces large dispersion for species selection.

ISBN 978-3-95450-169-4

For species selection with no loss in target species and preservation of beam quality, the CSS should: 1) be linearly achromatic; 2) generate large dispersion with small β_x (x-betatron lattice function) at collimation point to maximize selection resolution with vertical slits; and 3) output the beam with well-controlled envelopes for downstream transport. Requirements (1) and (3) can be met in an idealized linear optic limit with a symmetric beam envelope in the CSS by exploiting mirror symmetry about the axial mid-point of the CSS (strength of each element equals that of its mirror counterpart) and setting $D' = \alpha_x = \alpha_y = 0$ (D = dispersion function and $\alpha = -\beta'/2$) at the mid-point. The axisymmetric initial beam envelope conditions are adjusted to satisfy requirement (2) and achieve an "attractive" beam envelope devoid of large excursions.

The CSS design procedure was carried out with the code MADX [11] using a hard-edge lattice. Results are shown in Fig. 1. The lattice is achromatic with zero initial ($D_{in} = D'_{in} = 0$) and final dispersion ($D_{out} = D'_{out} = 0$), and the envelopes are symmetric about mid-plane with lattice functions satisfying $\beta_{\rm in} = \beta_{\rm out}$ and $\alpha_{\rm in} = -\alpha_{\rm out}$ to ideally recover axisymmetry on exit. The 1m-long 90-degree dipoles have slanted poles that generate a focusing strength equivalent to a superimposed quad with $\kappa_0 = 0.365$ m^{-2}. The electrostatic quadrupoles (ESQs) have axial length 20.7 cm with $\kappa_1 = 6.62$ m^{-2}, $\kappa_2 = -14.8$ m^{-2} and $\kappa_3 = 7.80$ m^{-2}. The initial envelope has $\beta_{\rm in} = 4.383$ m and $\alpha_{\rm in} = 0.306$, which we find (see below) are consistent with upstream matching from the ECR.

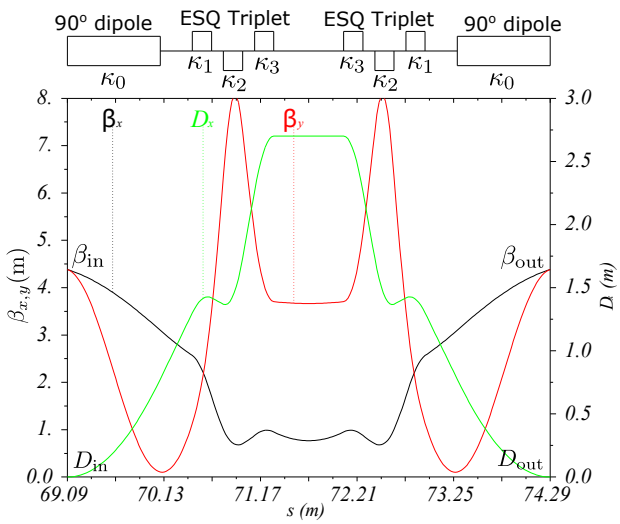

Figure 1: CSS lattice design used in Warp simulations.

The transport line from the ECR must be tuned to deliver the required lattice functions entering the CSS. We assume no initial centroid offset ($D_{in} = D'_{in} = 0$). Applying $\varepsilon_x = \varepsilon_{\rm eff}/2$, $\beta_x = \sigma_x^2/\varepsilon_x$ and $\alpha_x = -\sigma_x\sigma'_x/\varepsilon_x$ to convert between lattice functions and envelope size, the excitation of the two upstream solenoids are tuned to match the required lattice functions. Beam evolution in the axisymmetric transport line from the ECR to the 1st dipole of the CSS is described by a multi-species envelope equation:

$$\sigma''_{rj} = \frac{q_j V'}{2\mathcal{E}_{kj}}\sigma'_{rj} + \frac{q_j V''}{4\mathcal{E}_{kj}}\sigma_{rj} - \left(\frac{q_j B_{z0}}{2m_j\beta_{bj}c}\right)^2 \sigma_{rj} + \sum_{s,\,\text{species}} Q_{js} f_s \frac{\sigma_{rj}}{\sigma_{rj}^2 + \sigma_{rs}^2} + \frac{\varepsilon_{rj}^{\rm rms2} + \langle P_\theta\rangle_j^2 / \left(m_j\beta_{bj}c\right)^2}{\sigma_{rj}^3}. \quad (2)$$

Details of this model are in Ref. [7]. The canonical angular momentum measured by $\langle P_\theta\rangle/(m\beta c)$ contributes to the beam's expansion in the same manner as the thermal emittance $\varepsilon_r^{\rm rms}$ (related purely to ion temperature T), whereby

$$\varepsilon_{\rm eff}^2 = \varepsilon_{rj}^{\rm rms2} + \langle P_\theta\rangle_j^2 / \left(m_j\beta_{bj}c\right)^2 \quad (3)$$

constitutes an effective phase-space volume of the beam.

The envelope equation is numerically integrated along with an equation for the species energy using the linear fields extracted from the 3D element models. Figure 2 shows that the envelope equation achieves good agreement with Warp simulations both with and without space charge. Successively finer scans of the two solenoid fields (minimum increments being 0.002 Tesla) are carried out until target envelope conditions are matched.

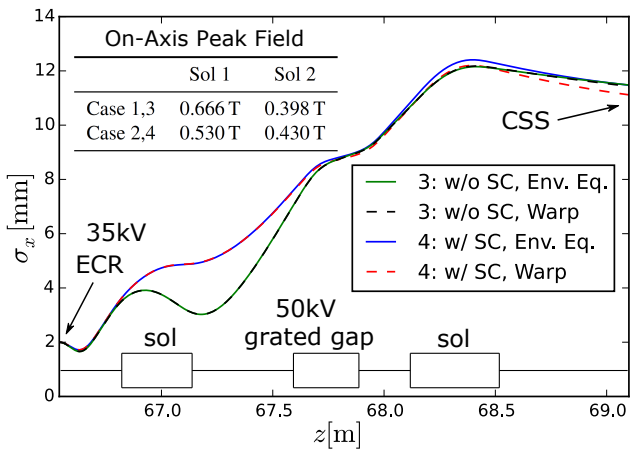

Figure 2: Comparisons between numerical solutions of the envelope equation and Warp simulation results in the transport line upstream of the CSS. These correspond to simulation cases 3 and 4 described below.

One caveat: the lattice design is not solely dictated by the CSS - in some cases the desired lattice functions are unattainable within the range of possible solenoid excitations. An alternative CSS operating point with attainable lattice functions must be selected in these cases!

Simulation Cases

Fields from lattice elements in the axisymmetric transport line are imported from Poisson [9] and CST Studio [10]. All elements in the CSS are modeled as hard-edge here to simplify comparisons to the MADX design lattice. Simulations with space charge include a uniform neutralization factor of 75% except inside the grated gap and the CSS lattice after the 1st dipole.

To illustrate effects of space charge and canonical angular momentum in the CSS, we launch beams with the same effective volume (ε_{eff}) as calculated from Eq. 3 but different compositions from thermal emittance and canonical angular momentum. A "magnetized" beam has phase space contributions consistent with Table 1 whereas the same volume is filled solely by thermal emittance in a "thermal" beam (i.e., increase T). The following cases were run: 1) No space charge, thermal beam; 2) case 1 with space charge; 3) no space charge, magnetized beam; and 4) case 3 with space charge. Note that case 4 is close to the lab expectation since canonical angular momentum dominates the effective phase space volume.

WARP SIMULATION RESULTS

Warp PIC simulations of the 4 cases in the CSS are contrasted to understand deviations from the MADX design due to space charge, non-constant emittance, canonical angular momentum, and nonlinear optical effects. Understanding the source of deviations will help optimize the CSS.

The rms beam envelope (Fig. 3a) and emittance (Fig. 3b) evolution of the reference species U^{34+}, and the centroid offset of U^{33+} along with mid-plane xy phase space projections (Fig. 3c) are shown. We observe the following behavior: a) beam rotation due to canonical angular momentum; b) in cases with space charge, non-reference species have centroid offset upon exiting the CSS; c) emittance growth which is mostly reversed; and d) emittance exchange between x and y for magnetized beams.

Distribution xy projections in Fig. 3c illustrate how a magnetized beam becomes tilted in real space at the CSS due to canonical angular momentum ($\langle P_\theta \rangle \neq 0$) whereas a thermal beam ($\langle P_\theta \rangle = 0$) does not. Large initial $\langle xy' \rangle$ and $\langle x'y \rangle$ moments in a magnetized beam causes $\langle xy \rangle$ to evolve in the non-axisymmetric lattice.

While space charge has little impact on the envelope evolution in x and y, insofar as the matching is carried out equivalently, the cases with and without space charge in Fig. 3c show that space charge creates a ~mm shift in the centroid of U^{33+}. Note that the canonical angular momentum affects neither the envelope size nor the dispersive shift.

Fig. 3b shows significant emittance growth inside the 1st bending dipole. This appears to be a consequence of nonlinear terms in the equation of motion becoming non-negligible due to large x/R_{bend}. The effect is stronger for thermal beams than for magnetized beams, regardless of space charge. For case 1-3 the growth appears reversible - the emittance undergoes a symmetric evolution in the 2nd dipole and almost recovers the original value upon exiting the CSS. Only the case of a magnetized beam with space charge exhibits emittance exchange between x and y in the CSS. The results suggest the exchange is generated by an interplay between these two effects. Understanding these effect and predicting the xy beam tilt angle should enable more effective choices of apertures and slit positions for species collimation.

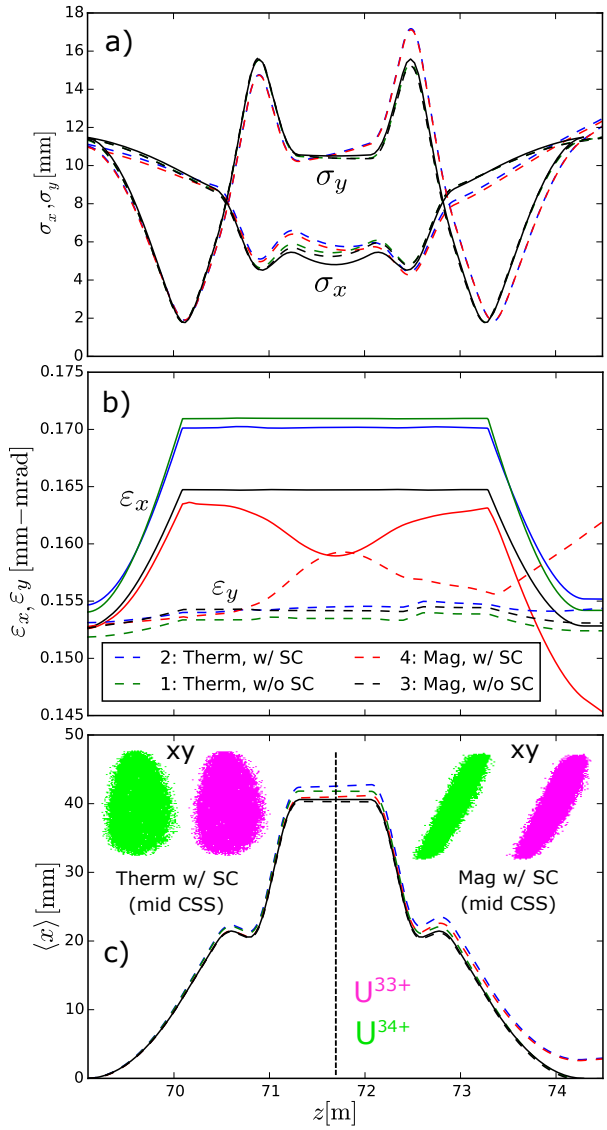

Figure 3: Rms envelops a) and normalized rms-emittance b) in x and y of the reference species U^{34+} in the CSS. c) shows the centroid of U^{33+} and xy-particle projections of both target species at the CSS mid-point for two cases. The black solid lines denote MADX design values in a) and c).

CONCLUSION

A framework of self-consistent PIC simulations is described, it will be applied to the commissioning ions and beamline to support early FRIB operations. Studies on the CSS uncovered effects such as xy beam rotation, emittance evolution and exchange, and space charge induced dispersion shift. There is ongoing work to improve beam collimation schemes consistent with these effects under increasing levels of model realism.

ACKNOWLEDGMENTS

Work supported by the U.S. DOE Office of Science under Cooperative Agreement DE-SC0000661 and the NSF under Grant No. PHY-1102511.

ISBN 978-3-95450-169-4

REFERENCES

[1] J. Wei *et al.*, "Progress at MSU towards a Facility for Rare Isotope Beams", in *Proc. NA-PAC'13*, Pasadena, CA, USA, November 2014, paper FRYBA3.

[2] J. Wei, "The FRIB Superconducting Linac - Status and Plans", presented at the LINAC'16, East Lansing, MI, USA, September 2016, paper M01A01, this conference.

[3] G. Machicoane, D. Cole, J. Ottarson, J. Stetson, P. A. Zavodszky, "ARTEMIS-B: A room-temperature test electron cyclotron resonance ion source for the National Superconducting Cyclotron Laboratory at Michigan State University", *Rev. Sci. Instrum.* 77, 03A322 (2006).

[4] D. Leitner, C.M. Lyneis, S.R. Abbott, D. Collins, R.D. Dwinell, M.L. Galloway, M. Leitner, and D.S. Todd, "Next generation ECR ion sources: First results of the superconducting 28GHz ECRIS–VENUS", *Nuclear Instruments and Methods in Physics Research Section* B **235**, pp.486-493 (2005).

[5] D. Leitner, T.J. Loew, C.M. Lyneis, I.C. Rodriguez, and D.S. Todd, 2008. "High intensity production of high and medium charge state uranium and other heavy ion beams with VENUS", *Rev. Sci. Instrum.* 79, 02C710 (2008).

[6] Warp web site, `http://warp.lbl.gov/` .

[7] S. M. Lund, E. Pozdeyev, H. Ren, and Q. Zhao, "RMS Emittance Measures for Solenoid Transport and Facility for Rare Isotope Beams Front-end Simulations", in *Proc. HB'14*, East Lansing, MI, USA, November 2014, paper MOPAB17.

[8] K. Fukushima, S. M. Lund , and C. Y. Wong, "MultiSpecies Simulation of the FRIB FrontEnd Near the ECR Sources with the Warp Code", presented at the LINAC'16, East Lansing, MI, USA, September 2016, paper TUPRC010, this conference.

[9] Poisson/Superfish web site, `http://laacg.lanl.gov/laacg/services/download_sf.phtml`

[10] CST Studio web site, `https://www.cst.com/products/csts2`

[11] MADX web site, `http://mad.web.cern.ch/mad/`

[12] S. M. Lund, T. Kikuchi, and R. C. Davidson,"Generation of Initial Kinetic Distribution for Simulation of Long-Pulse Charged Particle Beams with High Space-Charge Intensity", *Phys. Rev. ST Accel. Beams* **12** (2009) 114801.